

Combination therapy of lymphatic drug delivery and total body irradiation in a metastatic lymph node and lung mouse model

Shota Sora¹ | Ariunbuyan Sukhbaatar^{1,2}  | Shinichi Fukushima³  | Shiro Mori^{1,2} |
Maya Sakamoto^{1,2} | Tetsuya Kodama^{1,2} 

¹Laboratory of Biomedical Engineering for Cancer, Graduate School of Biomedical Engineering, Tohoku University, Sendai, Japan

²Biomedical Engineering Cancer Research Center, Graduate School of Biomedical Engineering, Tohoku University, Sendai, Japan

³Department of Metabolism and Diabetes, Graduate School of Medicine, Tohoku University, Sendai, Japan

Correspondence

Tetsuya Kodama, Laboratory of Biomedical Engineering for Cancer, Graduate School of Biomedical Engineering, Tohoku University, 4-1 Seiryō, Aoba, Sendai, Miyagi 980-8575, Japan.
Email: kodama@tohoku.ac.jp

Funding information

Japan Society for the Promotion of Science, Grant/Award Number: 20H00655, 20K20161, 21K18319 and 22K18203; Suzuken Memorial Foundation

Abstract

Chemotherapy using a lymphatic drug delivery system (LDDS) targeting lymph nodes (LNs) in the early stage of metastasis has a superior antitumor effect to systemic chemotherapy. An LDDS produces a higher drug retention rate and tissue selectivity in LNs. To expand the therapeutic coverage of LDDS from local treatment of metastatic LNs to prevention of distant metastases, the combination of treatment with therapies that enhance systemic tumor immune effects is an important therapeutic strategy. Recently, total body irradiation (TBI) has been shown to activate immune responses and alter the tumor microenvironment. Here we show that combination therapy with TBI and LDDS improves the antitumor effect of metastatic LNs and lung metastasis. Tumor cells were inoculated into the subiliac LN (SiLN) to induce metastasis into the proper axillary LN (PALN) and lung in a mouse model. TBI was carried out on day 4 after inoculation using a gamma irradiator. Lymphatic drug delivery into the accessory axillary LN was used to treat PALN. In vivo bioluminescence imaging, high-frequency ultrasound, and histology showed that combination therapy using TBI (total dose 1.0 Gy once) and the LDDS suppressed tumor growth in LNs and lung metastases and was more effective than using LDDS or TBI alone. Quantitative RT-PCR of spleens after combination therapy revealed increased expression of *CD4*, *CD8*, and *IL-12b*, indicating an activated immune response. The results show that combination therapy with TBI and LDDS is a method to improve the efficacy of LN metastases and distant metastases therapy and is a promising novel approach to treat cancer patients.

KEYWORDS

chemotherapy, cisplatin, lymph node metastasis, lymphatic drug delivery system, radiotherapy

Abbreviations: AALN, accessory axillary lymph node; CDDP, cisplatin; ICG, indocyanine green; IFN- γ , interferon γ ; Hsp, heat shock protein; IL, interleukin; LDDS, lymphatic drug delivery system; LN, lymph node; L-TBI, low-dose total body irradiation; M-TBI, middle-dose total body irradiation; PALN, proper axillary lymph node; qRT-PCR, quantitative RT-PCR; SiLN, subiliac lymph node; TBI, total body irradiation; Th1, T helper 1; TNF- α , tumor necrosis factor α .

This is an open access article under the terms of the [Creative Commons Attribution-NonCommercial](https://creativecommons.org/licenses/by-nc/4.0/) License, which permits use, distribution and reproduction in any medium, provided the original work is properly cited and is not used for commercial purposes.

© 2022 The Authors. *Cancer Science* published by John Wiley & Sons Australia, Ltd on behalf of Japanese Cancer Association.

1 | INTRODUCTION

Lymph node (LN) metastasis is a significantly poor prognostic factor for cancer patients.¹ Recently, the possibility of hematogenous distant metastasis has been proposed as “LN-mediated hematogenous metastasis theory,” in which tumor cells that reach the sentinel LN lymphatically proliferate in the marginal sinus and invade the veins perforating the LN and the surrounding area at the early stage of metastasis.^{2,3} Therefore, early treatment of nonenlarged false-negative LNs (i.e., clinical NO LNs), which are difficult to diagnose metastases with current clinical imaging equipment, will lead to not only better treatment of metastatic LNs but also the prevention of distant metastasis. Conventional treatments of metastatic LNs include LN dissection, systemic chemotherapy with hematogenous anticancer drugs, and radiation therapy.⁴ LN dissection is often undertaken on LNs that are metastatic and resectable (clinical N1 or greater), with the disadvantage that it is highly invasive, and there are multiple reports of surgical stress affecting postoperative tumor recurrence and immunosuppression.⁵⁻⁷

For systemic chemotherapy with hematogenous anticancer drugs, therapeutic effects on metastatic LNs are limited^{8,9} because of the lack of blood vessels and lymphatic vessels (perfusion defect formation),¹⁰⁻¹² non-angiogenesis,^{3,13} and increase in intranodal pressure in early metastatic LNs.

For radiation therapy of metastatic LNs, rather than a curative approach targeting micrometastasis in early metastatic LNs, the aim is to treat unresectable advanced metastatic LNs and to prevent LN metastasis within the irradiated field.

The LDDS is a local treatment method in which anticancer drugs are injected directly into LNs to target early metastases.¹⁴⁻¹⁶ The LDDS produces a higher drug retention rate and tissue selectivity in LNs compared to systemic chemotherapy and elicits greater antitumor effects.^{14,16} Assuming clinical application, the amount of drug used is extremely low (1/1000–10,000 of systemic chemotherapy), and side-effects are minimal. Recently, it has been shown that the antitumor effect can be further enhanced by adjusting the anticancer drugs used in LDDS with a highly osmotic, highly viscous solvent.^{14,16} To expand the therapeutic coverage of LDDS from local treatment of metastatic LNs to prevention of distant metastases, the combination of treatment with therapies that enhance systemic tumor immune effects is an important therapeutic strategy.

Numerous reports have found that total body irradiation (TBI) enhanced antitumor effects by inducing both innate and acquired immunity, and altering the immune system and tumor microenvironment.¹⁷⁻²⁶ Therefore, the combination therapy of TBI and LDDS is expected to be a new therapeutic strategy to treat micrometastases in early metastatic LNs and distant organs. In the present study, the efficacy of combination therapy with TBI and LDDS with high osmotic pressure and high viscosity anticancer drugs was clarified against LN metastases and distant metastases in a mouse model of metastasis without a primary tumor, thus eliminating the influence of the site and size of a primary tumor.

2 | MATERIALS AND METHODS

2.1 | Mice

Mouse experiments were carried out following ethical guidelines and approved by the Institutional Animal Care and Use Committee of Tohoku University.

MXH10/Mo-*lpr/lpr* (MXH10/Mo/*lpr*) mice (12–15 weeks old) were used in all experiments.²⁷ The mice develop enlarged LNs up to 10 mm in diameter at 2.5–3 months, and the size and onset time of the LN swelling was stable and predictable. There are two LNs in the axillary area; proper axillary LN (PALN) and accessory axillary LN (AALN). The AALN and SiLN are LNs located upstream of the PALN, and lymph flows from the AALN to the PALN, and from the SiLN to the PALN in one direction.²⁷

2.2 | Tumor inoculation and metastasis induction

C3H/He mouse mammary carcinoma (FM3A-Luc) cells, which express the luciferase gene²⁷ were used. Cells were cultured in 10% (v/v) FBS (Funakoshi), to which 1% (v/v) L-glutamine-penicillin-streptomycin (Sigma-Aldrich) and 0.5 mg/ml G418 (Sigma-Aldrich) was added. The medium was changed every 4–5 days. Cells were used in experiments after three passages. Lack of *Mycoplasma* contamination was confirmed on the inoculation day (MycAlert Mycoplasma Detection Kit; Lonza Rockland). FM3A-Luc cells (3.3×10^5 cells/ml; 19,800 cells/60 μ l), suspended in a mixture of 20 μ l PBS and 40 μ l of 400 mg/m Matrigel (Collaborative Biomedical Products), were injected into the SiLN to induce metastasis in the PALN and lungs.

2.3 | Total-body irradiation, chemotherapy with LDDS, and combination therapy with TBI and LDDS

Mice were divided into four groups to compare therapeutic effects: LDDS group ($n = 5$), Single M-TBI group ($n = 7$), Single M-TBI + LDDS group ($n = 5$), and Nontreatment group ($n = 6$). Tumor cells were injected into SiLNs and TBI was carried out on day 4 (4 days after inoculation; Figure 1A).

A gamma irradiator (Gammacell 40 Exactor; Best Theratronics) equipped with two opposing cesium-137 (¹³⁷Cs) sources was used for TBI. In a preliminary experiment, the inhibition of tumor growth of LN metastases and distant metastases was compared between the Single L-TBI group ($n = 6$) that received a single low dose (0.2 Gy) of TBI and the Single M-TBI group ($n = 7$) that received a single middle dose (1.0 Gy) of TBI. The Single M-TBI group showed better-suppressed growth of metastatic tumors in the PALN and lung compared to the Single L-TBI group (Figures S1 and S2). Therefore, in the present study, a single M-TBI was used with an average dose rate of 0.769 Gy/min cumulative 1.0 Gy (1 min 18 s).

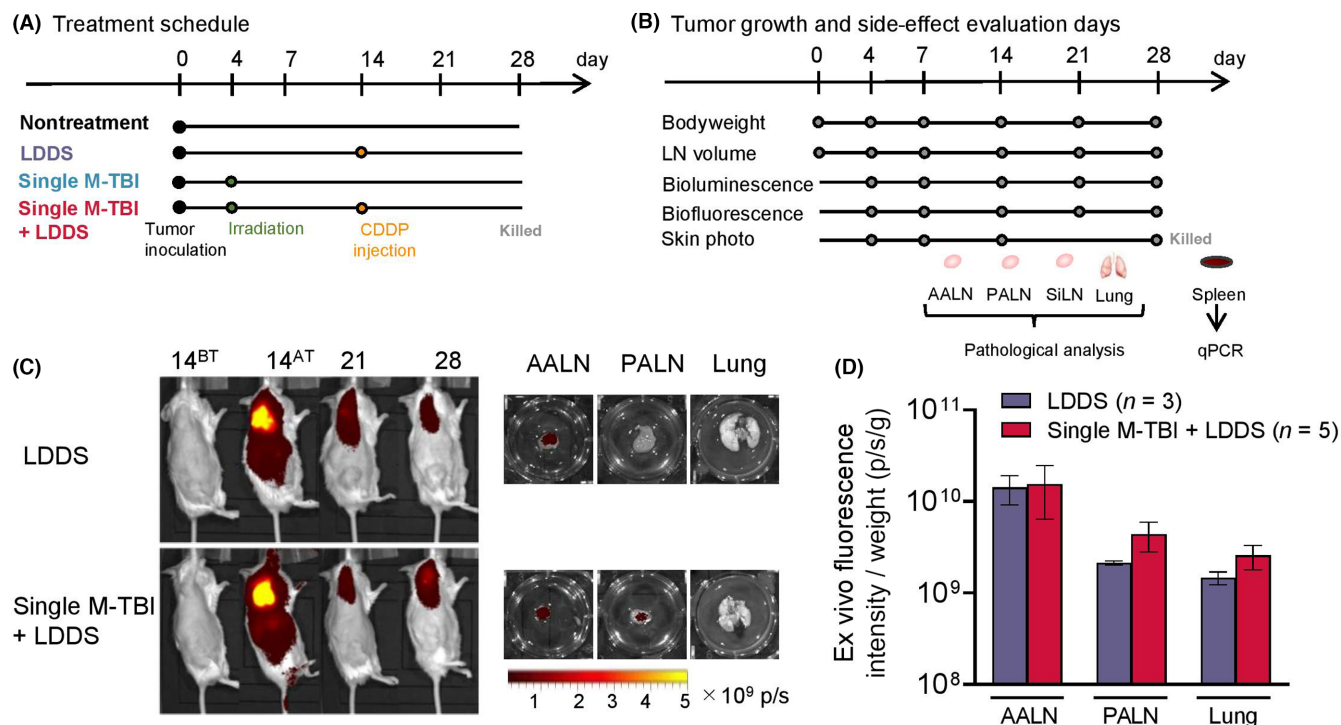


FIGURE 1 Experimental schedule for TBI and LDDS with cisplatin and flow dynamics and retention of ICG. (A) Day 0 was set as the day of direct bolus administration of 60 μ l FM3A-Luc cell suspension into SiLNs. (B) Tumor growth and drug retention were evaluated by measuring the bioluminescence intensity over time. LN volume was measured over time. Mice were sacrificed on day 28 and histopathological and genetic analyses carried out. (C) Cisplatin mixed with ICG was injected into the SiLN, and in vivo ICG fluorescence intensity images were measured over time. Ex vivo ICG fluorescence intensity images of AALN, PALN, and lung, removed on day 28. (D) Ex vivo ICG fluorescence intensity per weight in AALN, PALN, and lung. LDDS group, $n = 3$; Single M-TBI+LDDS group, $n = 5$. In the LDDS and Single M-TBI+LDDS groups, high in vivo ICG fluorescence intensity was observed around the AALN and PALN on day 14 immediately after drug injection and decreased over time. The ex vivo bioluminescence intensity of LNs and organs removed on day 28 was higher in AALN, PALN, and lung, in this order, confirming that the drug reached and accumulated in the LNs, and lung. 14^{AT}, 14 days after treatment; 14^{BT}, 14 days before treatment; qPCR, quantitative PCR

The experimental groups that were given drugs through the LDDS were the LDDS and the Single M-TBI+LDDS groups.

In these groups, the AALN on the same side as the SiLN inoculated with the tumor cells 14 days after inoculation (day 14) was treated with 200 μ l CDDP at a concentration of 5 mg/kg, which is the upstream LN to the PALN (Figure 1A). Based on a previous study that showed that CDDP with high osmolality and high viscosity delivered through the LDDS was effective in inhibiting metastatic tumor growth,¹⁴ CDDP was adjusted to an osmotic pressure of 1897 kPa and a viscosity of 11.5 mPa-s, using a solution of polysorbate 80 (NOF), saline (Otsuka Pharmaceutical Factory), 100% ethanol (Fujifilm Wako), distilled water, and 100 μ g/ml indocyanine green (ICG) solution (Daiichi Sankyo Co., Ltd). To evaluate the biodistribution and retention of the administered drug, ICG (molecular weight, 775; excitation wavelength, 774 nm; emission wavelength, 805 nm) was mixed with cisplatin solution, and in vivo ICG fluorescence intensity was measured using an in vivo bioluminescence imaging system (IVIS; PerkinElmer, Inc.) on days 14, 21, and 28 after drug treatment. On day 28, the AALN, PALN, and lung were resected, and the ex vivo ICG fluorescence intensity per organ weight was measured.

2.4 | Evaluation of tumor growth

The inhibitory effect of metastatic tumor growth in the Single M-TBI, LDDS, Single M-TBI+LDDS, and Nontreatment groups was evaluated by bioluminescence intensity (Figure 1B). A bioluminescence imaging system (IVIS; PerkinElmer, Inc.) was used for bioluminescence image acquisition and bioluminescence intensity measurements. The in vivo bioluminescence intensity was calculated per unit time using the provided analysis software (Living Image; PerkinElmer). The bioluminescence intensity on each measurement day after the intervention was normalized to the bioluminescence intensity on day 4. The right AALN, PALN, and lung were resected on day 28 and ex vivo bioluminescence images and bioluminescence intensity measurements of the LNs and the organs were made.

2.5 | Lymph node volume measurement

Tumor growth in LNs and the inhibitory effect of tumor growth after treatment were investigated by measuring the LN volume

using a high-frequency ultrasound imaging system for small animals (VEVO770; Fujifilm Visual Sonics). B-mode 2D images of PALN were acquired on days 0, 4, 7, 14, 21, and 28, and 3D images were reconstructed using VEVO software (V3.0.0; Fujifilm Visual Sonics) (Figure 1B). LN volumes were calculated from 3D images of the LNs, and the LN volumes on each measurement day and after treatment intervention were normalized based on the LN volume of the PALN on day 0. The changes in LN volumes in the Single M-TBI, LDDS, Single M-TBI+LDDS, and Nontreatment groups were compared.

2.6 | Bodyweight measurement

Mice were weighed on days 0, 4, 7, 14, 21, and 28 and compared between the Single M-TBI, LDDS, Single M-TBI+LDDS, and Nontreatment groups.

2.7 | Observation of skin changes induced by TBI

On days 4, 7, 14, and 28, macro photographs of mouse skin surfaces were taken to evaluate skin damage caused by TBI in the Single M-TBI and Single M-TBI+LDDS groups.

2.8 | Histological analyses

PA LNs, AALNs, SiLNs, and lungs, removed on day 28 (Figure 1B), were embedded in paraffin and thin sections (2.5 μm) were prepared. PA LNs, AALNs, and SiLNs were stained with Hematoxylin Eosin (H&E), and lungs were stained with H&E and Elastica Masson's stain.^{6,7} Histopathological findings of PALNs and lungs of the Single M-TBI, LDDS, Single M-TBI+LDDS, and Nontreatment groups were analyzed.

2.9 | Quantitative RT-PCR

Spleens in the Single M-TBI, LDDS, Single M-TBI+LDDS, and Nontreatment groups were removed from mice 28 days after tumor cell inoculation, and total RNAs were isolated with a FastGene RNA Premium Kit (Nippon Genetics Co., Ltd). Each aliquot of 2 μg total RNA was reverse transcribed to synthesize cDNA using a High Capacity cDNA Reverse Transcription Kit (Applied Biosystems) according to the manufacturer's instructions. The expression levels of cell surface antigens (*CD4*, *CD8*), cytokines (*IL-6*, *IL-12b*, *TNF- α* , *IFN- γ*), and heat shock proteins (*Hsp70*, *Hsp90*) were measured by qRT-PCR using an ABI 7500 Real-Time PCR System (Applied Biosystems). Expression of *GAPDH* was used as the internal control. The nucleotide sequences for primers and probes are listed in Table S1. Amplifications were carried out in 15 μl reaction mixtures in triplicate using ABsolute qPCR ROX Mix (Thermo Fisher Scientific) according to the manufacturer's recommended method. The expression of target genes relative to *GAPDH* expression was calculated

as follows: $2^{-\Delta(\text{dCT})}$ ($\text{dCt} = \text{Ct} [\text{target}] - \text{Ct} [\text{GAPDH}]$). Independent triplicate assays were carried out.

2.10 | Statistical analysis

The results of in vivo bioluminescence intensity, ex vivo bioluminescence intensity, LN volume, and bodyweight changes are given as the mean \pm SEM. The Bliss independence model was used to analyze the drug and radiation combination therapy effect in the PALN (model constructed in the Excel module of Microsoft Office 365), and data are presented as percentages \pm SEM.

Statistical analysis software (GraphPad Prism 8; GraphPad Software, Inc.) was used to evaluate significant differences and for graphing. One-way ANOVA, Tukey's multiple comparison test, two-way ANOVA, Tukey's multiple comparison test, and an uncorrelated *t*-test were used for significance tests. The results at **** $p < 0.0001$, *** $p < 0.001$, ** $p < 0.01$, and * $p < 0.05$ are considered to be statistically significant differences.

3 | RESULTS

3.1 | Evaluation of drug delivery and retention using ICG fluorescence intensity measurements

In the LDDS and Single M-TBI+LDDS groups, the drug was immediately delivered from the AALN to the total body after injection into the AALN, and showed high in vivo ICG fluorescence intensity around the AALN and PALN. The ICG fluorescence intensity reached a maximum on day 14 after treatment and then decreased over time (Figure 1C).

The ex vivo bioluminescence intensity of LNs and organs resected on day 28 was higher in the order of AALN, PALN, and lung, indicating that the drug reached and accumulated not only in LNs but also in the major organs. There was no statistically significant difference between the LDDS and the Single M-TBI+LDDS groups in ex vivo ICG fluorescence intensity per weight of AALN, PALN, or lung (Figure 1D).

3.2 | In vivo evaluation of tumor growth by bioluminescence intensity

The bioluminescence intensity of SiLNs, which are tumor cell inoculation sites showing luciferase activity, increased over time in the Nontreatment, LDDS, Single M-TBI, and Single M-TBI+LDDS groups (Figure 2A). Bioluminescence intensity in metastatic PALN and lung was lower in the LDDS, Single M-TBI, and Single M-TBI+LDDS groups than in the Nontreatment group on day 14 (Figure 2A–C). Bioluminescence intensity in the PALN and lung on day 28 was statistically significantly lower in the Single M-TBI and Single M-TBI+LDDS groups compared to the Nontreatment group (Figure 2C)

3.3 | Ex vivo bioluminescence intensity

Ex vivo bioluminescence in PALN was detected throughout the LNs in the Nontreatment and LDDS groups, and only locally in the Single M-TBI and Single M-TBI+LDDS groups (Figure 2A). The ex vivo bioluminescence intensity of the PALN was lowest in the

Single M-TBI+LDDS group, followed by the Single M-TBI group and the LDDS group, and all these groups showed significantly lower levels than the Nontreatment group (Figure 2D). The ex vivo bioluminescence intensity in the lungs of the Nontreatment and LDDS groups showed localized bioluminescence (Figure 2A). In contrast, no bioluminescence was detected in the lungs of the

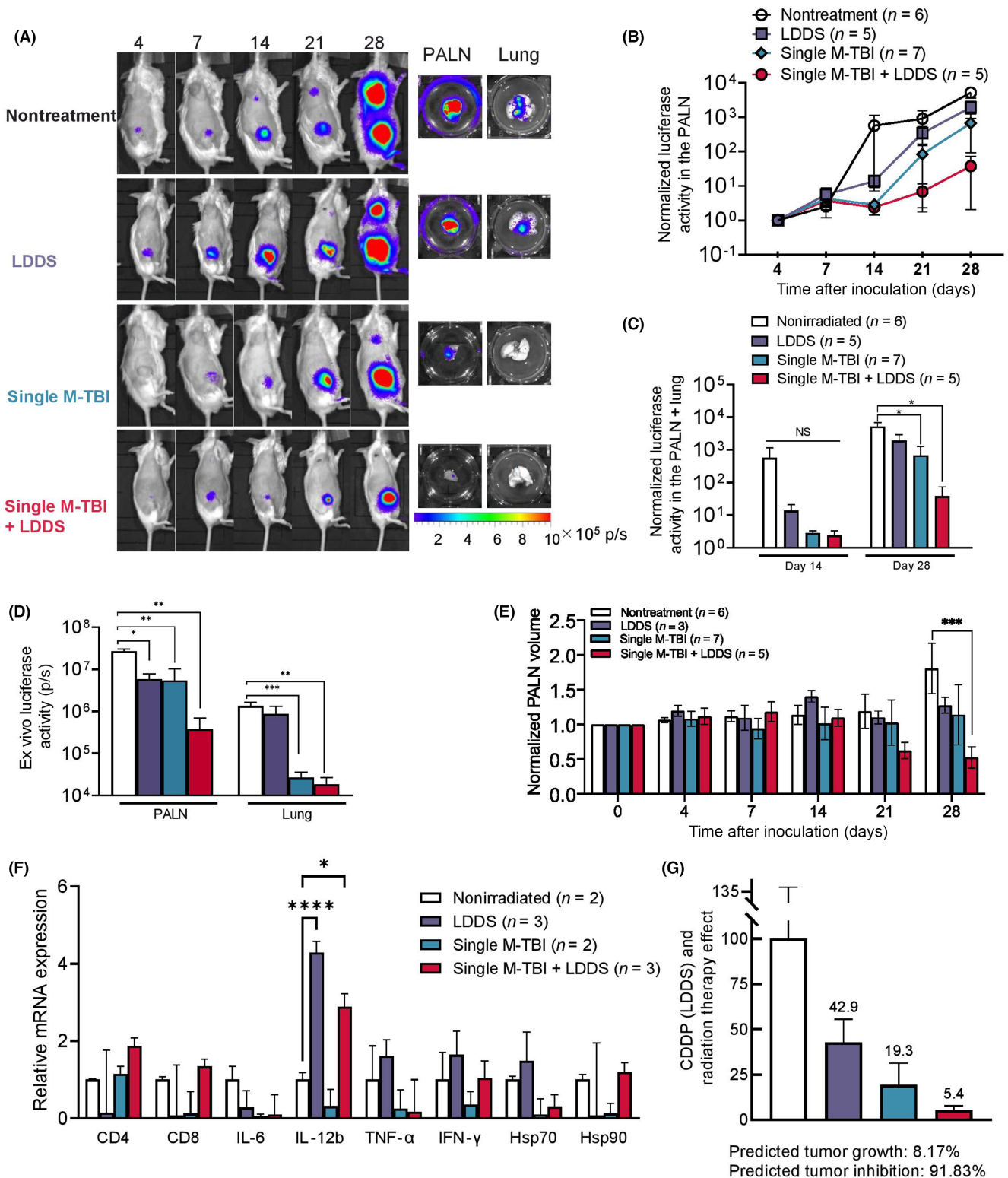


FIGURE 2 Legend on next page

FIGURE 2 Tumor inhibition using a combination of Single M-TBI and LDDS. (A) In vivo bioluminescence intensity images over time after injection of anticancer drugs to AALN. Ex vivo bioluminescence intensity images of PALN, and lung on day 28 after LDDS alone, Single M-TBI, and Single M-TBI+LDDS. (B) In vivo bioluminescence intensity over time normalized to day 4 of LDDS alone, LDDS and Single M-TBI+LDDS in the PALN and lung region. (C) Normalized in vivo bioluminescence intensity of PALN and lung on day 14 (before LDDS treatment) and on day 28. The bioluminescence intensity of PALN on day 28 was statistically significantly lower in the Single M-TBI ($n = 7$) and Single M-TBI+LDDS ($n = 5$) groups compared to the Nontreatment group ($n = 6$), indicating that tumor growth was suppressed. (D) Ex vivo bioluminescence intensity in PALN and lung. Ex vivo bioluminescence in PALN was attenuated in the Single M-TBI and Single M-TBI+LDDS groups. The ex vivo bioluminescence intensity was lowest in the Single M-TBI+LDDS group and significantly lower in all treatment groups compared to the Nontreatment group. The ex vivo bioluminescence intensity in the lungs was also significantly lower in the treated groups compared to the Nontreatment group. (E) The PALN volume on day 28 was statistically significantly lower than that of the Nontreatment group ($n = 6$). LDDS group, $n = 3$; Single M-TBI group, $n = 7$; Single M-TBI+LDDS group, $n = 5$. (F) Quantitative RT-PCR. Expression levels of cell surface antigens, cytokines, and heat shock proteins (Hsp) in spleen. In the LDDS group ($n = 3$), *IL-12b*, *TNF- α* , *IFN- γ* , and *Hsp70* levels were upregulated compared to the Nontreatment group ($n = 2$), the upregulation of *IL-12b* being especially significant. *CD4*, *CD8*, *IL-6*, and *Hsp90* levels were downregulated. In the Single M-TBI group ($n = 2$), only the expression level of *CD4* was upregulated compared to the Nontreatment group. In the Single M-TBI+LDDS group ($n = 3$), the expression levels of *CD4*, *CD8*, *IL-12b*, *IFN- γ* , and *Hsp90* were upregulated compared to the Nontreatment group. (G) Tumor inhibition. Tumor growth was found to be 42.9% for LDDS alone, 19.3% for Single M-TBI, and 5.4% for Single M-TBI+LDDS whereas tumor inhibition was 57.1%, 80.7%, and 94.6%, respectively. * $p < 0.05$, ** $p < 0.01$, *** $p < 0.001$, **** $p < 0.0001$. NS, not significant

Single M-TBI or Single M-TBI+LDDS groups, and the intensity was statistically significantly lower than that of the Nontreatment group (Figure 2A,D)

3.4 | Metastatic LN volume changes

The PALN volume increased over time in the Nontreatment group, while no obvious change was observed in the LDDS or Single M-TBI groups. In contrast, the PALN volume in the Single M-TBI+LDDS group decreased over time and the PALN volume on day 28 was statistically significantly lower than that of the Nontreatment group (Figure 2E).

3.5 | Quantitative RT-PCR and whole-body findings

Figure 2F shows the mRNA expression levels of cell surface antigens (*CD4*, *CD8*), cytokines (*IL-6*, *IL-12b*, *TNF- α* , *IFN- γ*), and heat shock proteins (*Hsp70*, *Hsp90*) measured by qRT-PCR in spleens resected from mice after treatments. In the LDDS group, *IL-12b*, *TNF- α* , *IFN- γ* , and *Hsp70* were upregulated compared to the Nontreatment group, the upregulation of *IL-12b* being especially significant. However, *CD4*, *CD8*, *IL-6*, and *Hsp90* were downregulated. In the Single M-TBI group, the expression level of *CD4* was upregulated compared to that in the Nontreatment group, but the expression levels of *CD8*, *CD6*, *IL-12b*, *TNF- α* , *IFN- γ* , *Hsp70*, and *Hsp90* were all downregulated. In the Single M-TBI+LDDS group, the expression levels of *CD4*, *CD8*, *IL-12b*, *IFN- γ* , and *Hsp90* were upregulated compared to the Nontreatment group.

Figure 2G shows predicted tumor growth and predicted tumor inhibition. Single M-TBI+LDDS was inhibited tumor growth effectively among these groups. The Single M-TBI+LDDS, LDDS, and Single M-TBI groups showed no significant weight loss after treatment compared to the Nontreatment group. In addition, no

inflammatory changes in the skin or pneumonia were detected in any of the TBI mice.

3.6 | Histopathological analysis

The results of histopathological analyses of the PALN and lungs in the Nontreatment, LDDS, Single M-TBI, and Single M-TBI+LDDS groups are shown in Figure 3. In the H&E-stained specimens of PALN, tumors were widely distributed throughout the PALN in the Nontreatment and LDDS groups (Figure 3A, a–d). In the Single M-TBI group, no tumor was found in the parenchyma, but tumors remained in and around the marginal sinus (Figure 3A, e,f). In the Single M-TBI+LDDS group, there were PALNs with no tumor in the LNs (Figure 3A, g,h) and PALNs with the tumor in and around the marginal sinus (Figure 3A, i,j).

In H&E-stained specimens of AALN, necrosis of lymphoid tissues was observed in the LDDS and Single M-TBI+LDDS groups. In PALNs without tumors in the Single M-TBI+LDDS group, necrosis was observed in the parenchyma. In contrast, in the PALN without tumor in the Single M-TBI+LDDS group, necrosis was observed around the export lymphatic vessels of the AALN in addition to the parenchyma. In the lungs, tumors were observed in the Nontreatment group (Figure 3B, a,b), but not in the LDDS, Single M-TBI, or Single M-TBI+LDDS groups (Figure 3B, c–h). There was also no evidence of pneumonia in any of the groups.

4 | DISCUSSION

This is the first experimental report showing that the combination therapy of M-TBI (1.0 Gy) and LDDS with CDDP is effective in the treatment of LN metastasis and distant metastasis in an LN metastasis mouse model. TBI is a technique used to treat several diseases including multiple myeloma, leukemias, lymphomas, and some solid tumors.²⁸ It remains an effective myeloablative therapy, particularly

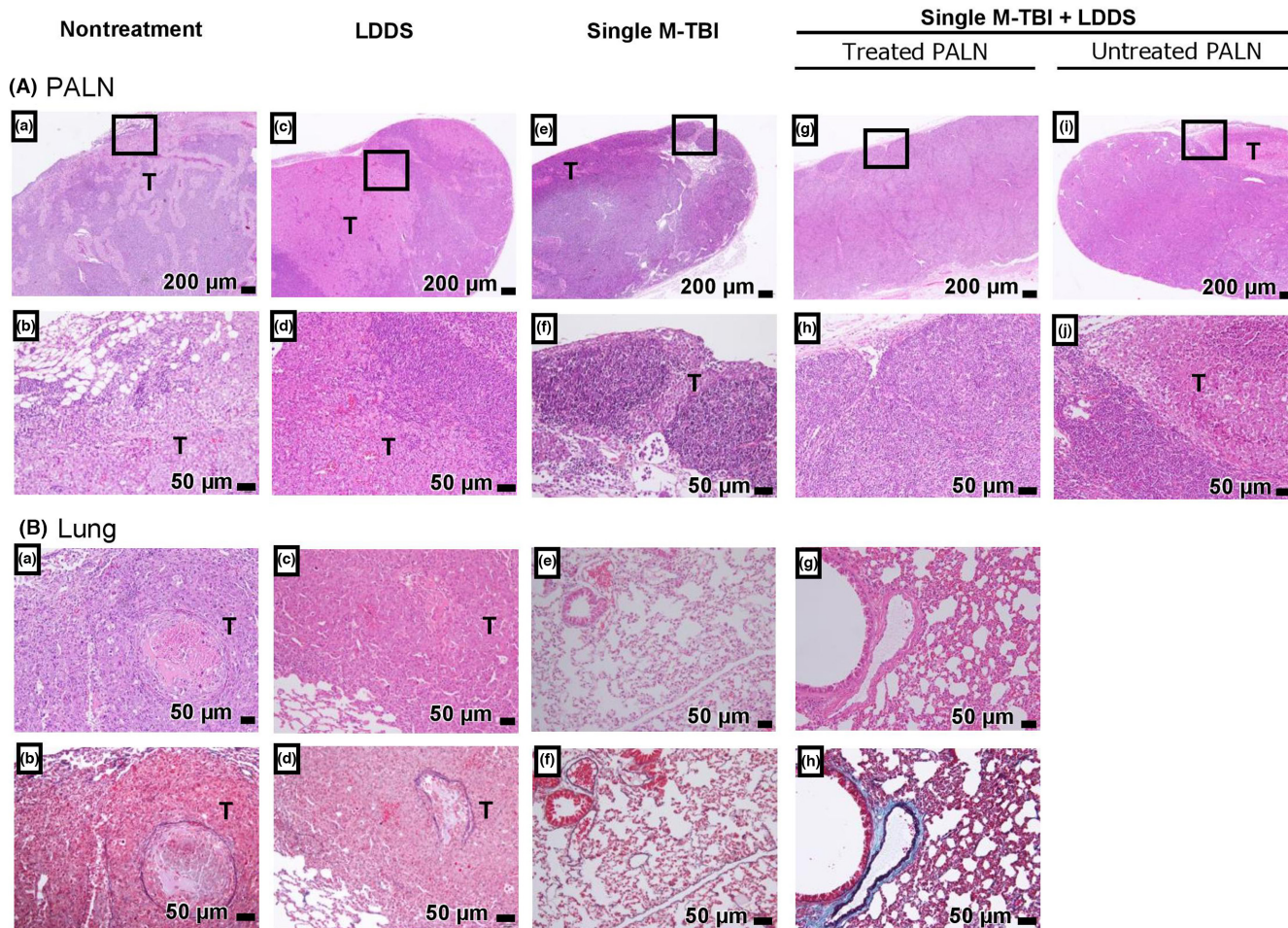


FIGURE 3 Histopathological analyses. (A) Histopathological analysis of PALN (H&E staining). (a, b) Nontreatment group, (c, d) LDDS group, (e, f) Single M-TBI group, (g–j) Single M-TBI + LDDS group. Panels b, d, f, h, and j are enlarged views of the regions indicated in panels a, c, e, g, and i. Tumors were widely distributed throughout the PALN in the Nontreatment and LDDS groups, whereas in the Single M-TBI group tumors remained only in and around the marginal sinus. In the Single M-TBI + LDDS group, some tumors were located in the PALN, while others were located in and around the marginal sinus. (B) Histopathological analysis of lung (H&E and Elastica Masson's staining). (a, b) Nontreatment group, (c, d) LDDS group, (e, f) Single M-TBI group, (g, h) Single M-TBI + LDDS group. In the lungs, tumors were observed in the Nontreatment group, but not in the LDDS, Single M-TBI, or Single M-TBI + LDDS groups. T, tumor

in regimens used for preparation and conditioning prior to allogeneic stem cell transplantation for leukemia. The total dose was 12 Gy with fractionated irradiation.²⁹

Many previous studies have shown that TBI activates antitumor immunity. TBI induces activation of innate immune responses (natural killer cells, macrophages, and dendritic cells) and adaptive immune responses (CD4 and CD8) for antitumor immunity, and promotes the release of inflammatory cytokines and cytokines involved in antitumor immunity.³⁰ Peritoneal macrophages show an M1 phenotype and increased secretion of IL-12 and IL-18 in mice exposed to a single M-TBI.³¹ IFN- γ and IL-12 produced by macrophages can induce antigen-presenting naïve CD4⁺ T (Th0) cells to differentiate into Th1 cells, enhancing Th1 cell-mediated antitumor effects.^{32,33}

Anticancer drugs not only provide antitumor effects, but also reduce immune function and could eliminate endogenous factors of cancer cells, the tumor microenvironment, and cancer lesions. However, depending on the dose and schedule of anticancer drugs,

chemotherapy has been found to have a direct immunostimulatory effect by increasing the maturation and cytotoxic potential of specific immune cell populations.³⁴ Chemotherapy-induced immunogenic modulation of anticancer drugs and immunogenic cell death should be regarded as the result of a spectrum of immunogenic cell stress, not as separate events.³⁵ Cisplatin is structurally and functionally similar to oxaliplatin, but its slight difference in structure induces different levels of immunogenic cell stress,³⁵ leading to immunogenic cell death.³⁶ Direct administration of CDDP into LNs by LDDS is an effective method to increase bioavailability in LNs and to induce immunogenic cell stress.^{14,16}

In the present study, the expression level of CD4 was upregulated in the Single M-TBI group and Single M-TBI + LDDS group compared to the Nontreatment group, and downregulated in the LDDS group compared to the Nontreatment group (Figure 2F). In other words, it is considered that Single M-TBI induced activation of CD4⁺ T cells and ameliorated the LDDS-induced decrease in CD4.

In contrast, *IL-12b*, *TNF- α* , *IFN- γ* , and *Hsp70* were upregulated in the LDDS group compared to the Nontreatment group, indicating that LDDS alone activates antitumor immunity. The expression levels of *CD4*, *CD8*, *IL-12*, and *Hsp90* were upregulated in the Single M-TBI+LDDS group compared to the Nontreatment group, suggesting that both Single M-TBI and LDDS alone can activate different antitumor immunity and improve both the antitumor effect through Th1 cells and the antitumor immune response through CD8.

In addition, tumor growth was found to be 42.9% for LDDS, 19.3% for single M-TBI, and 5.4% for single M-TBI+LDDS groups, whereas tumor inhibition was 57.1%, 80.7%, and 94.6%, respectively (Figure 2G). In addition, we found lower percentages of predicted tumor growth and tumor inhibition in the single M-TBI+LDDS groups, indicating that the combination of these treatment methods had a synergistic effect (Figure 2G).

In preliminary experiments, the same qRT-PCR was undertaken in the L-TBI group and the Single M-TBI group to compare the expression levels of cell surface antigens (*CD4*, *CD8*), cytokines (*IL-6*, *IL-12a*, *IL-12b*, *TNF- α* , *IFN- γ*), and heat shock proteins (*Hsp70*, *Hsp90*). The expression levels of heat shock proteins (*Hsp70* and *Hsp90*) were compared in the Single L-TBI group. In the Single L-TBI group, *CD4*, *CD8*, *IL-6*, *IL-12b*, *TNF- α* , *IFN- γ* , and *Hsp70* were upregulated compared to the Nontreatment group, whereas only *CD4* was upregulated in the Single M-TBI group (Figure S1F). These results suggest that the combination of low-dose TBI and LDDS enhances the antitumor immune response more than a combination of Single M-TBI and LDDS. The radiation dose should be as low as possible and the antitumor immune response should be high. Limitations of this paper include: the most appropriate dose for TBI chosen and when anticancer drugs should be administered to activate antitumor immunity and inhibit tumor growth.

Further detailed studies are required to determine whether fractionated irradiation using TBI and multiple doses of drugs through the LDDS will improve the therapeutic anticancer effects.

This is the first study to quantitatively determine the therapeutic efficacy of TBI or the combination of TBI and LDDS for the treatment of metastatic LNs and LN-mediated lung metastasis. Combination therapy with TBI and LDDS can inhibit metastatic tumor growth in LNs and the lung without significant side-effects, and is expected to be an effective therapy with potential clinical applications for human cancer patients in the near future.

AUTHOR CONTRIBUTIONS

TK: conceptualization, methodology, validation, project administration, review and editing, supervision, funding acquisition. MS: writing original draft and supervision. SM: histopathological analysis, supervision, review and editing. SF: supervision and editing. AS: preparation of images, formal analysis, validation, writing – review and editing, supervision, funding acquisition. SS: investigation, data curation, formal analysis, visualization.

ACKNOWLEDGMENTS

The study was supported by JSPS KAKENHI grant numbers 20K20161 (AS), 22K18203 (AS), 20H00655 (TK), and 21K18319 (TK). Suzuken Memorial Foundation (AS).

DISCLOSURE

The authors declare that they have no competing interests.

ETHICS STATEMENT

Approval of the research protocol by an Institutional Review Board: 2019BeA-011-06.

ANIMAL STUDIES

Guidelines of the Institutional Animal Care and Use Committee of Tohoku University, which conform to the provisions of the Declarations of Helsinki and ARRIVE guidelines, were complied with for all investigations carried out using mouse models.

ORCID

Ariunbuyan Sukhbaatar  <https://orcid.org/0000-0001-9137-2966>

Shinichi Fukushige  <https://orcid.org/0000-0003-0588-6376>

Tetsuya Kodama  <https://orcid.org/0000-0003-4727-9558>

REFERENCES

- Alexandrescu ST, Selaru FM, Diaconescu AS, et al. Prognostic value of lymph node ratio in patients with resected synchronous colorectal liver metastases and less than 12 examined lymph nodes. *J Gastrointest Surg.* 2022;26:141-149.
- Kodama T, Mori S, Nose M. Tumor cell invasion from the marginal sinus into extranodal veins during early-stage lymph node metastasis can be a starting point for hematogenous metastasis. *Journal of Cancer Metastasis and Treatment.* 2018;4:56.
- Takeda K, Mori S, Kodama T. Study of fluid dynamics reveals direct communications between lymphatic vessels and venous blood vessels at lymph nodes of mice. *J Immunol Methods.* 2017;445:1-9.
- Ryan GM, Kaminskas LM, Porter CJ. Nano-chemotherapeutics: maximising lymphatic drug exposure to improve the treatment of lymph-metastatic cancers. *J Control Release.* 2014;193:241-256.
- Deboever N, McGrail DJ, Lee Y, et al. Surgical approach does not influence changes in circulating immune cell populations following lung cancer resection. *Lung Cancer.* 2022;164:69-75.
- Sukhbaatar A, Mori S, Saiki Y, Takahashi T, Horii A, Kodama T. Lymph node resection induces the activation of tumor cells in the lungs. *Cancer Sci.* 2019;110:509-518.
- Sukhbaatar A, Sakamoto M, Mori S, Kodama T. Analysis of tumor vascularization in a mouse model of metastatic lung cancer. *Sci Rep.* 2019;9:16029.
- Torchilin V. Tumor delivery of macromolecular drugs based on the EPR effect. *Adv Drug Deliver Rev.* 2011;63:131-135.
- Nune SK, Gunda P, Majeti BK, Thallapally PK, Forrest ML. Advances in lymphatic imaging and drug delivery. *Adv Drug Deliv Rev.* 2011;63:876-885.
- Iwamura R, Sakamoto M, Mori S, Kodama T. Imaging of the mouse lymphatic sinus during early stage lymph node metastasis using intranodal lymphangiography with X-ray micro-computed tomography. *Mol Imaging Biol.* 2019;21:825-834.
- Yamaki T, Sukhbaatar A, Mishra R, et al. Characterizing perfusion defects in metastatic lymph nodes at an early stage using high-frequency ultrasound and micro-CT imaging. *Clin Exp Metastasis.* 2021;38:539-549.
- Sakamoto M, Kojima I, Iikubo M, et al. Perfusion defects in non-enlarged metastatic lymph nodes using vessel wall magnetic resonance imaging: detection performance and diagnostic value. *Clin Exp Metastasis.* 2022;39:421-431.
- Mikada M, Sukhbaatar A, Miura Y, et al. Evaluation of the enhanced permeability and retention effect in the early stages of lymph node metastasis. *Cancer Sci.* 2017;108:846-852.

14. Fukumura R, Sukhbaatar A, Mishra R, Sakamoto M, Mori S, Kodama T. Study of the physicochemical properties of drugs suitable for administration using a lymphatic drug delivery system. *Cancer Sci.* 2021;112:1735-1745.
15. Kato S, Yoshida S, Mori S, Kodama T. Optimization of the delivery of molecules into lymph nodes using a lymphatic drug delivery system with ultrasound. *Int J Pharm.* 2021;597:120324.
16. Sukhbaatar A, Mori S, Kodama T. Intranodal delivery of modified docetaxel: innovative therapeutic method to inhibit tumor cell growth in lymph nodes. *Cancer Sci.* 2022;113:1125-1139.
17. Janiak MK, Wincenciak M, Cheda A, Nowosielska EM, Calabrese EJ. Cancer immunotherapy: how low-level ionizing radiation can play a key role. *Cancer Immunol Immunother.* 2017;66:819-832.
18. Zhou L, Zhang X, Li H, et al. Validating the pivotal role of the immune system in low-dose radiation-induced tumor inhibition in Lewis lung cancer-bearing mice. *Cancer Med.* 2018;7:1338-1348.
19. Bogdandi EN, Balogh A, Felgyinszki N, et al. Effects of low-dose radiation on the immune system of mice after total-body irradiation. *Radiat Res.* 2010;174:480-489.
20. Italiani P, Boraschi D. From monocytes to M1/M2 macrophages: phenotypical vs functional differentiation. *Front Immunol.* 2014;5:514.
21. Kojima S. Induction of glutathione and activation of immune functions by low-dose, whole-body irradiation with gamma-rays. *Yakugaku Zasshi.* 2006;126:849-857.
22. Liu R, Xiong S, Zhang L, Chu Y. Enhancement of antitumor immunity by low-dose total body irradiation associated with selectively decreasing the proportion and number of T regulatory cells. *Cell Mol Immunol.* 2010;7:157-162.
23. Liu J, Zhou J, Wu M, et al. Low-dose Total body irradiation can enhance systemic immune related response induced by hypofractionated radiation. *Front Immunol.* 2019;10:317.
24. Richaud PM, Soubeyran P, Eghbali H, et al. Place of low-dose total body irradiation in the treatment of localized follicular non-Hodgkin's lymphoma: results of a pilot study. *Int J Radiat Oncol Biol Phys.* 1998;40:387-390.
25. Safwat A, Bayoumy Y, El-Sharkawy N, Shaaban K, Mansour O, Kamel A. The potential palliative role and possible immune modulatory effects of low-dose total body irradiation in relapsed or chemo-resistant non-Hodgkin's lymphoma. *Radiother Oncol.* 2003;69:33-36.
26. Tanaka Y, Komori H, Mori S, et al. Evaluating the role of rheumatoid factors for the development of rheumatoid arthritis in a mouse model with a newly established ELISA system. *Tohoku J Exp Med.* 2010;220:199-206.
27. Shao L, Mori S, Yagishita Y, et al. Lymphatic mapping of mice with systemic lymphoproliferative disorder: usefulness as an inter-lymph node metastasis model of cancer. *J Immunol Methods.* 2013;389:69-78.
28. Wills C, Cherian S, Yousef J, Wang K, Mackley HB. Total body irradiation: a practical review. *Appl Radiat Oncol.* 2016;5:11-17.
29. Wong JYC, Filippi AR, Dabaja BS, Yahalom J, Specht L. Total body irradiation: guidelines from the international lymphoma radiation oncology group (ILROG). *Int J Radiat Oncol Biol Phys.* 2018;101:521-529.
30. Verma NK, Fazil M, Duggan SP, Kelleher D. Combination therapy using inhalable GapmeR and recombinant ACE2 for COVID-19. *Front Mol Biosci.* 2020;7:197.
31. Wu Q, Allouch A, Martins I, Modjtahedi N, Deutsch E, Perfettini JL. Macrophage biology plays a central role during ionizing radiation-elicited tumor response. *Biom J.* 2017;40:200-211.
32. Rackov G, Tavakoli Zaniani P, Colomo del Pino S, et al. Mitochondrial reactive oxygen is critical for IL-12/IL-18-induced IFN- γ production by CD4+ T cells and is regulated by Fas/FasL signaling. *Cell Death Dis.* 2022;13:531.
33. Ue H, Rafiq M, Khawar MB, Nazir B, Haider G, Nazir N. The multifaceted role of IL-12 in cancer. *Adv Cancer Biol Metast.* 2022;5:100053.
34. Shurin MR, Naiditch H, Gutkin DW, Umansky V, Shurin GV. ChemolmmunoModulation: immune regulation by the antineoplastic chemotherapeutic agents. *Curr Med Chem.* 2012;19:1792-1803.
35. Fabian KP, Wolfson B, Hodge JW. From immunogenic cell death to immunogenic modulation: select chemotherapy regimens induce a Spectrum of immune-enhancing activities in the tumor microenvironment. *Front Oncol.* 2021;11:728018.
36. Galluzzi L, Humeau J, Buque A, Zitvogel L, Kroemer G. Immunostimulation with chemotherapy in the era of immune checkpoint inhibitors. *Nat Rev Clin Oncol.* 2020;17:725-741.

SUPPORTING INFORMATION

Additional supporting information can be found online in the Supporting Information section at the end of this article.

How to cite this article: Sora S, Sukhbaatar A, Fukushige S, Mori S, Sakamoto M, Kodama T. Combination therapy of lymphatic drug delivery and total body irradiation in a metastatic lymph node and lung mouse model. *Cancer Sci.* 2023;114:227-235. doi: [10.1111/cas.15562](https://doi.org/10.1111/cas.15562)